Tropospheric Delay Effects in Radio Interferometry

G. Lanyi
Tracking Systems and Applications Section

A new tropospheric mapping function is derived which is more accurate than previous mapping functions above elevations of 4 degrees. The error due to the given analytic approximation is estimated to be less than 0.02% for elevation angles larger than 6 degrees, (less than 0.4 cm at 6 degrees, and approximately 0.004% or 0.03 cm at 20 degrees). The mathematical expansion used in the derivation is valid for any laterally homogeneous atmospheric model of refractivity. The new mapping function, computer generated ray tracing tables and other mapping functions are compared. The results can be used in correcting for tropospheric delays of radio signals.

I. Introduction

Radio waves traversing the atmosphere of the earth are delayed due to electromagnetic refraction. The delay depends on the length of the path; consequently, it is a function of the incident elevation angle of the radio wave. Usually, since satellite and stellar radio sources are observed only above 6° elevation, we set our precision requirements at 6°. The primary causes for this low elevation angle limit are: antenna pointing limits, ground obstructions, system noise and signal multipathing. In addition, modeling errors of the tropospheric delay are relatively large at very low elevation angles.

The tropospheric delay at an (unrefracted) elevation angle E can be determined by the mapping function $s(E)$. If the Earth's atmosphere is approximated by a laterally homogeneous plane air layer and the refractive bending of the ray is neglected, then $s(E) = Z/\sin E$, where Z is the zenith delay.

The mean sea level value for the dry tropospheric delay is ~2.3 m at zenith and ~20 m at 6° elevation. The delay of 20 m is a mean delay value for a laterally homogeneous dry atmosphere. Spherical geometry and refraction bending effects are included in the delay. For $E = 6°$, $1/\sin E \sim 9.6$; thus the difference between the mean and the approximated (plane air layer) delay is ~−2 m and it is smaller at higher elevation angles, approximately given by $-\epsilon Z/(\sin E \tan^2 E)$. This effect is primarily due to the curvature of the air layer. The mean value for ϵ is ~0.00122. This functional form for the delay correction was first derived by Saastamoinen (Ref. 1). The proportionality factor ϵ is a function of the atmospheric model of refractivity. Thus a 10% modeling error in ϵ results in an ~20 cm delay error at 6° elevation. Consequently, mismodelings of the tropospheric mapping can cause significant errors at low elevation angles.

In addition to the errors resulting from inherent zenith delay uncertainties, there are errors due to mismodelings, inhomogeneities and large-scale temporal variations. The corresponding major delay errors at low elevation angles are the following:

(1) Refractive bending.

(2) Dry modeling errors.

(3) Water vapor variations.

The refractive bending effect is ~13 cm at 6° elevation and can be completely removed by proper modeling. The variation of the bending effect due to zenith delay changes is ~20% or 2-3 cm at 6°. The dry and wet errors are about 10 and 11 cm, respectively, and these errors correspond to 1-2 σ estimates. The dry errors are due primarily to variations of the temperature profile of the troposphere. The water vapor errors are due primarily to large-scale temporal variations (e.g., diurnal variations) and inhomogeneities. In the estimate of the wet variations, a 6 hour observation period is assumed.

In the following, the effect of these errors in radio interferometric measurements will be discussed and we will describe a relatively accurate tropospheric delay function, which aids in removing some of these errors.

II. Tropospheric Delay Errors in Radio Interferometry

The delay errors described in Section I may occur in radio interferometric measurements. The present formal accuracy level of various interferometric measurements varies between 0.1 and 10 cm, depending on the baseline length and the number of observations. These formal accuracy figures do not account for all the systematic errors. Systematic errors can be incorrectly absorbed into parameter estimates. The magnitude of the error for estimates of intercontinental baselines is about the size of the delay errors estimated in Section I. Observations at low elevation angles are, however, necessary on long baselines for the following reasons:

(1) The visibility of radio sources by two stations is limited.

(2) Good geometry requires well separated multiple observations of radio sources.

(3) Such observations enable better determinations of zenith delay or other model parameters.

Direct experimental verifications of tropospheric delay errors are often difficult. A statistical evaluation of elevation dependent post-fit residuals may be used for indirect verification. However, elevation dependent systematics can be caused by other effects also. The major sources of error are ionospheric delays and antenna cable delays. Dual band ionospheric calibration results in small calibration errors. Antenna cable delays may have a different elevation dependence, and we do not have well established magnitude estimates for the Deep Space Network antennas at present. There are indications, however, that the effect does not exceed 15 cm in magnitude (L. E. Young, private communication, 1980) and antenna cable delay errors, in principle, are removed by proper calibration techniques. Consequently, a large portion of elevation dependent systematic errors may be caused by tropospheric delay errors. Elevation dependent systematics were reported by Treuhaft[1], Treuhaft et al. (Ref. 2), Treuhaft, Lanyi, and Sovers (Ref. 3), Shapiro et al. (Ref. 4), and Davis, Herring and Shapiro (Ref. 5).

Treuhaft[1] (see also Ref. 3) introduced a statistical measure for testing the elevation-angle dependence of the post-fit residuals for the 1978-1983 Deep Space Network Very Long Baseline Interferometry (VLBI) data. This test indicated a statistically significant elevation dependence for the data set. Treuhaft's other results indicate that the systematics persist for different tropospheric mapping functions with constant temperature model parameters. Additional results showed that elevation dependent systematics can be induced by simulations of temporal tropospheric variations.

III. Computational Approach

The tropospheric delay expression has to be a function of all major atmospheric model parameters if precise corrections for atmospheric changes are necessary. The first task is to establish an atmospheric model of the refractivity. Refractivity models of dry air can be relatively accurate. However, there is no accurate model for the highly variable water vapor.

For a given refractivity model one can evaluate the actual tropospheric delay by two different computational approaches:

(1) Computerized numerical calculation, i.e., ray tracing.

(2) Analytic formulation and approximation.

The first approach is relatively straightforward but time-consuming. This feature is particularly amplified when tropospheric parameters are varied. The second approach results in relatively fast computation, and, as a byproduct, it gives more insight into the problem than the previous approach. Analytic formulations were given by Hopfield (Refs. 6 and 7), Saastamoinen (Ref. 1), Chao (Ref. 8), Marini and Murray (Ref. 9), Black (Ref. 10), Black and Eisner (Ref. 11), and Lanyi[2] (see also Ref. 12).

For the dry air, the assumptions of static equilibrium and the ideal gas law are basically sufficient to describe the dry

[1]Treuhaft, R. N., "Time Variation of Intercontinental Baselines Using VLBI: Analysis and Validation," IOM 335.1-176, January 1984, private communication.

[2]Lanyi, G., "Tropospheric Propagation Delay Effects for Radio Waves," IOM 335.1-156, November 15, 1983, private communication.

refractivity profile if the temperature profile of the atmosphere is known. We use a temperature profile consisting of three linear sections. In former work one- or two-section profiles were used. For the water vapor, Saastamoinen's semi-empirical model is applied (Ref. 1).

In the analytic approximation we expand the tropospheric delay up to the third order in refractivity. The second and third order terms describe the refractive bending effect. These higher order terms were not explicitly included in former tropospheric mapping functions. Other expansions are carried out in parameters related to the curvature of the Earth's surface, e.g., the scale height divided by the local radius of curvature. Using these approximations we integrate over the curved path of the ray (see Fig. 1) and obtain the formula given in Appendix B. The derivation is not given here, but detailed calculations and other considerations will be presented in another publication.

The tropospheric delay formula given in Appendix B can be easily computer coded. We performed computerized ray tracing also for comparing various analytic mapping functions. Using the mean atmospheric parameters listed in Appendix A, we obtained comparison plots (see Figs. 2 through 4). These plots show that for the given atmospheric parameters the new mapping function is very close to the ray tracing result. For a different set of atmospheric parameters the other mapping functions might approach more closely the ray tracing in certain elevation regions, but the fundamental discrepancies cannot be removed.

IV. Summary

The tropospheric delay formula presented in Appendix B is a relatively accurate expression as far as the model and the derivation are concerned. The zenith delays and temperature profile parameters may be obtained from meteorological data. Alternatively, under some experimental circumstances, certain model parameters can be estimated from the data itself. In radio interferometric experiments on long baselines, total or individual (dry or wet) tropospheric zenith delays can be relatively well estimated if observations with low elevation angles are included in the experiment.

The major error, which cannot be estimated from the experiment, is due to water vapor inhomogeneities. This error is ~ 6 cm at 6° elevation. The temporal and azimuthal variations of the water vapor are also difficult to estimate from the experiment itself. Consequently, precise line-of-sight measurements by water vapor radiometers may be necessary to determine the delay due to water vapor. For this purpose, we assume that the total error for the water vapor radiometer is smaller than the errors we seek to eliminate. However, water vapor radiometers, in general, are not designed to function accurately at low elevation angles; thus the path toward high precision could be a difficult one.

As far as experimental verification of the new mapping function is concerned, two initial results should be mentioned:

(1) The new mapping function with fixed mean temperature profile parameters is statistically preferred by our data (Ref. 3). This is the same data set as was mentioned in Section II for antenna stations in Australia, California and Spain for the full 5 year period. The station in Australia has some bias, though, and sites at other geographical locations might have also somewhat different mean temperature profile parameters and correspondingly different mapping functions.

(2) Elevation dependent systematics can be partially removed by using variable atmospheric model parameters (Ref. 3).

Both findings are initial results.

In conclusion, it would seem that the best approach for determining the tropospheric delay function parameters lies in the combined use of surface and radiosonde meteorological data, water vapor radiometer data and statistical model parameter estimates.

References

1. Saastamoinen, J., Atmospheric Correction for the Troposphere and Stratosphere in Radio Ranging of Satellites, The Use of Artificial Satellites for Geodesy, Geophysical Monograph 15, American Geophysical Union, Washington, D. C., 1972.

2. Treuhaft, R. N., Liewer, K. M., Niell, A. E., Sovers, O. J., Thomas, J. B., and Wallace, K. S., The Time Variation of Intercontinental Baselines Using VLBI: Analysis and Validation, EOS Transactions, American Geophysical Union, Washington, D. C., 64, 678, 1983.

3. Treuhaft, R. N., Lanyi, G. E., and Sovers, O. J., Empirical Troposphere Modeling from DSN Intercontinental VLBI Data, EOS Transactions, American Geophysical Union, 65, 191, 1984.

4. Shapiro, I. I., et al., Geodesy by Radio Interferometry: Interpretation of Intercontinental Distance Measurements, EOS Transactions, American Geophysical Union, 64, 677, 1983.

5. Davis, J. L., Herring, T. A., and Shapiro, I. I., Geodesy by Radio Interferometry: Effects of Errors in Modeling the Troposphere, EOS Transactions, American Geophysical Union, 65, 191, 1984.

6. Hopfield, H. S., Two-quartic Troposphere Refractivity Profile for Correcting Satellite Data, J. Geophys. Res., 74, 4487-4499, 1969.

7. Hopfield, H. S., Tropospheric Effect on Electromagnetically Measured Range: Prediction from Surface Weather Data, Radio Sci., 6, 357-367, 1971.

8. Chao, C. C., The Tropospheric Calibration Model for Mariner Mars 1971, Tracking System Analytic Calibration Activities for the Mariner Mars 1971 Mission, Technical Report 32-1587, 61-76, Jet Propulsion Laboratory, Pasadena, California, March 1974.

9. Marini, J. W., and Murray, C. W., Correction of Laser Range Tracking Data for Atmospheric Refraction at Elevations above 10 degrees, NASA/GSFC X-591-73-351, 1973.

10. Black, H. D., An Easily Implemented Algorithm for the Tropospheric Range Correction, J. Geophys. Res., 83(B4), 1825-1828, 1978.

11. Black, H. D., and Eisner, A., Correcting Satellite Doppler Data for Tropospheric Effects, J. Geophys. Res., 89(D2), 2616-2626, 1984.

12. Lanyi, G. E., Tropospheric Propagation Delay Effects in Radio Interferometric Measurements, EOS Transactions, American Geophysical Union, 64, 210, 1983.

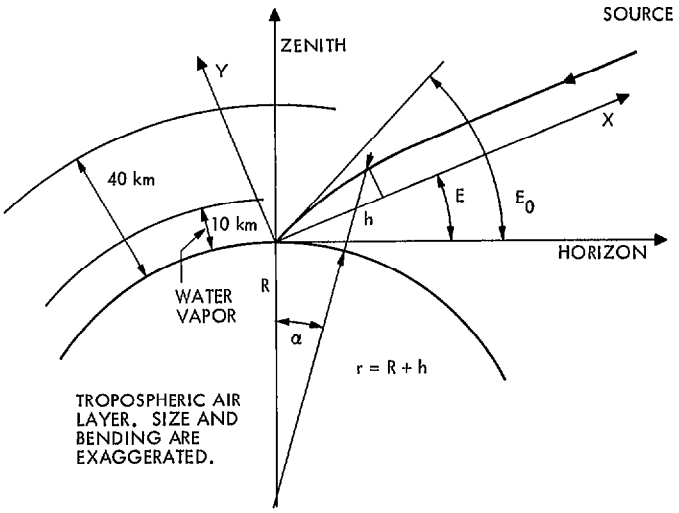

Fig. 1. Tropospheric refraction

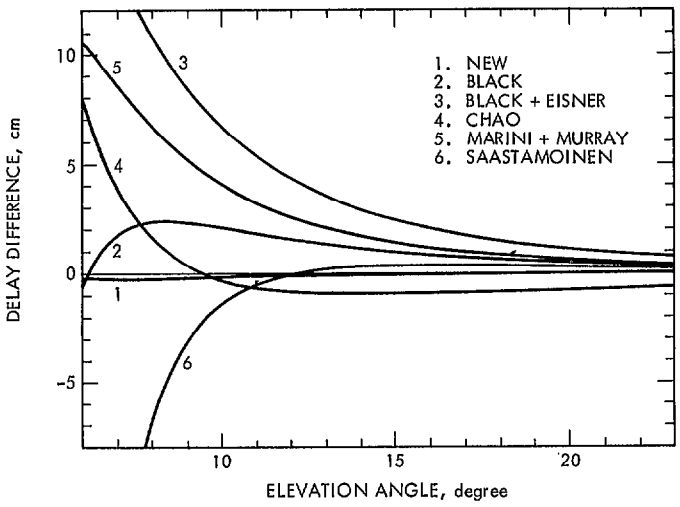

Fig. 3. Difference between the mapping functions and ray tracing for elevation angles of 6°–20°

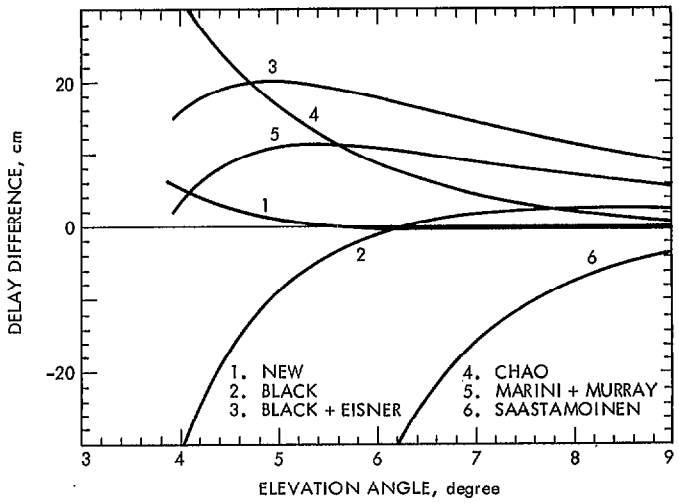

Fig. 2. Difference between the mapping functions and ray tracing for elevation angles of 4°–9°

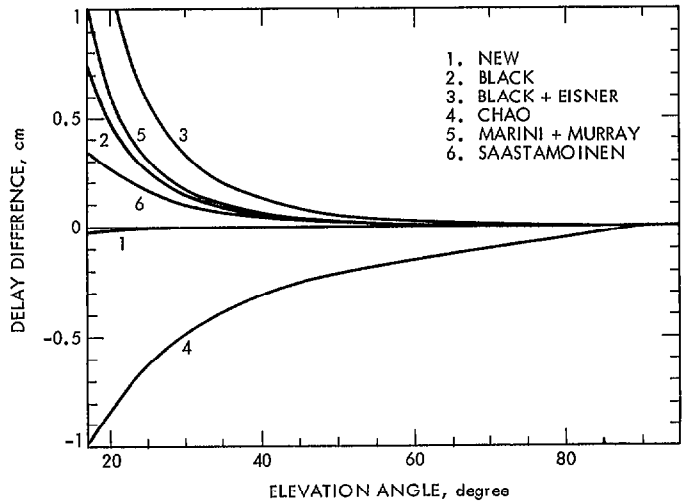

Fig. 4. Difference between the mapping functions and ray tracing for elevation angles of 20°–90°

Appendix A
List of Symbols

This is a list of symbols used in the tropospheric delay formula (see Appendix B). The values given here were used for calculating the plots in Figs. 2 through 4. The values of model parameters are chosen such that different models would match each other as closely as possible. Since the models can be matched only in an approximate manner, the values given here are the results of a compromise.

E	(unrefracted)	elevation angle
$s(E)$		tropospheric delay mapping function
p_0	= 1013.25 mbar (sea level)	surface pressure
T_0	= 292K	surface temperature
R	= 6371 km (for matching models)	radius of curvature of Earth
θ	= 45°	latitude
m	= 4.8097 10^{-23}g (dry air)	mean molecular mass
k	= 1.38066 10^{-16}erg/K	Boltzmann's constant
k/m	= 2.8706 10^{6} erg/gK	a gas constant of dry air
g_c	= 978.37 erg/g • cm	gravity at the center of gravity of air column
w	= 6.8165 K/km (a mean value)	temperature lapse rate
α	= 5 ($\alpha = mg_c/kw$, Hopfield's and Chao's value)	dry model parameter
β	= 3.5 (a mean value)	wet model parameter
h_1	= 0 (for matching models)	inversion altitude
h_2	= 12.2 km (Chao's value)	tropopause altitude
Z_{wet}	= 0 (for matching models)	wet zenith delay
λ	= 1 for $E > 10°$, = 3 for $E < 10°$	a scale factor

From the values above we obtain:

Δ	= 8.567 km ($\Delta = kT_0/mg_c$)	scale height
σ	= 1.345 10^{-3} ($\sigma = \Delta/R$)	a curvature measure
q_1	= 0 (scale height-normalized)	inversion altitude
q_2	= 1.424 (scale height-normalized)	tropopause altitude
Z_{dry}	= 230.70 cm	dry zenith delay

Appendix B

Tropospheric Delay

The tropospheric delay is the difference between the actual and a hypothetical vacuum (straight line) propagation time of the radio signal. In principle, by applying Fermat's principle for a laterally homogeneous spherical air layer, the path of the radio signal can be derived. The path is a function of the constant of integration. After expressing the constant of integration as a function of the unrefracted elevation angle E, an integration of the refractivity over the path is carried out. This gives the total propagation delay. After subtracting the vacuum delay, the tropospheric delay $s(E)$ is obtained.

These steps cannot be carried out exactly in an analytic fashion. The tropospheric delay formula presented in this appendix is a result of numerous approximations. The resultant tropospheric delay is a function of dry and wet zenith delays, Z_{dry} and Z_{wet}. The dry and wet zenith delays can be predicted from meteorological data (see, e.g., Ref. 1) or from the experiment itself. The tropospheric delay is also a function of other temperature profile related parameters: Δ, σ, α, q_1, q_2. The parameter β is a semi-empirical model parameter for the refractivity of the water vapor. The definition of the symbols and a set of mean values are given in Appendix A. These parameters can be adjusted according to local meteorological conditions.

In the following equations we use the indices d and w for referring to certain integrals of dry and wet surface-normalized refractivities, respectively. The index dw refers to the integrals of the product of dry and wet surface-normalized refractivities.

The tropospheric delay can be written as:

$$s(E) = F(E)/\sin E \tag{1}$$

Expansions in the refractivity and other quantities result in:

$$\begin{aligned} F(E) = {} & Z_{dry}F_{dry}(E) + Z_{wet}F_{wet}(E) + (Z^2_{dry}/\Delta)\,F_{bend1}(E) \\ & + 2\,(Z_{dry}Z_{wet}/\Delta)\,F_{bend2}(E) + (Z^2_{wet}/\Delta)\,F_{bend3}(E) \\ & + (Z^3_{dry}/\Delta^2)\,F_{bend4}(E) \end{aligned} \tag{2}$$

where

$$F_{dry}(E) = G(\lambda\langle q\rangle_d,u)A_d(E) + (3/4)G^3(\langle q\rangle_d,u)\langle q^2\rangle_d u\sigma \tag{3}$$

$$F_{wet}(E) = G(\lambda\langle q\rangle_w/\langle q^0\rangle_w,u)A_w(E)/\langle q^0\rangle_w \tag{4}$$

and

$$\left.\begin{aligned} F_{bend1}(E) = {} & -\frac{1}{2\tan^2 E}\left[G^3\left(\frac{\{q\}_d}{\{q^0\}_d},u\right)\{q^0\}_d - G^3(\langle q\rangle_d,u)\,\frac{\sigma}{\sin^2 E}\right] \\ F_{bend2}(E) = {} & -\frac{1}{2\tan^2 E}\,G^3\left(\frac{\{q\}_{dw}}{\{q^0\}_{dw}},u\right)\frac{\{q^0\}_{dw}}{\langle q^0\rangle_w} \\ F_{bend3}(E) = {} & -\frac{1}{2\tan^2 E}\,G^3\left(\frac{\{q\}_w}{\{q^0\}_w},u\right)\frac{\{q^0\}_w}{\langle q^0\rangle^2_w} \\ F_{bend4}(E) = {} & -\frac{1}{2\tan^4 E}\,G^3\left(\frac{\{\{q\}\}}{\{\{q^0\}\}},u\right)\{\{q^0\}\}_d \end{aligned}\right\} \tag{5}$$

The quantity $G(q,u)$ is a geometric factor related to the curvature of the Earth's surface and given by

$$G(q,u) = (1+qu)^{-1/2} \tag{6}$$

where

$$u = 2\sigma/\tan^2 E \tag{7}$$

The quantity $A(E)$ is given by

$$A(E) = \langle q^0\rangle + \sum_{n=1}^{10} ((2n-1)!!/n!)(-1/2)^n\,[u/1+\lambda\langle q\rangle u]^n\ \langle (q-\lambda\langle q\rangle)^n\rangle \tag{8}$$

The indices d and w in $A_d(E)$ and $A_w(E)$ refer to dry and wet moments in Eq. (8). The moments $\langle (q-\lambda\langle q\rangle)^n\rangle$ can be evaluated in terms of the moments $\langle q^n\rangle$ by the use of the binomial theorem. The quantities $\langle q^n\rangle$, $\{q^n\}$ and $\{\{q^n\}\}$ are the n-th order moments of the surface-normalized dry/wet refractivity $f(q), f^2(q)$ and $f^3(q)$,

$$
\left.
\begin{aligned}
\langle q^n \rangle &= \int_0^\infty dq\, q^n f(q) \\
\{q^n\} &= \int_0^\infty dq\, q^n f^2(q) \\
\{q^n\}_{dw} &= \int_0^\infty dq\, q^n f_{\text{dry}}(q) f_{\text{wet}}(q) \\
\{\{q^n\}\} &= \int_0^\infty dq\, q^n f^3(q)
\end{aligned}
\right\} \qquad (9)
$$

Denoting all the six types of dry, wet, and bend moments by $[q^n]$, for the particular three-section temperature profile model, we have

$$
\begin{aligned}
[q^n] = n!\, [&(1/a)^{n+1} (1 - \exp(-aq_1)) \\
&+ \exp(-aq_1) \left(\prod_{i=0}^{n} (\alpha/(b+i+1)) \right) (1 - \hat{T}_2^{b+n+1}(q_2)) \\
&+ (1/a)^{n+1} \exp(-aq_1)\, \hat{T}_2^{b+n+1}(q_2)]
\end{aligned} \qquad (10)
$$

where a and b are listed in the following table:

a	b		$[q]$
1	$\alpha - 1$	dry	$\langle q \rangle_d$
β	$\beta\alpha - 2$	wet	$\langle q \rangle_w$
2	$2\alpha - 2$	dry squared	$\{q\}_d$
$\beta + 1$	$\beta(\alpha + 1) - 3$	product of dry and wet	$\{q\}_{dw}$
2β	$2\beta\alpha - 4$	wet squared	$\{q\}_w$
3	$3\alpha - 3$	dry cubed	$\{\{q\}\}_d$

and

$$
\hat{T}_2(q_2) = 1 - (q_2 - q_1)/\alpha \qquad (11)
$$

If we set $q_1 = 0$ and neglect the bending terms and the second term in the dry expression, set $A(E) = 1$ and $\lambda = 1$ in the dry and wet formulas, and expand $G(\langle q \rangle, u)$, retaining the first order term for the dry and zeroth order term for the wet mapping function, then Saastamoinen's mapping function is obtained.

If we set $q_1 = 0$, $q_2 = 5$, and $\alpha = 5$, neglect the bending terms, set $A(E) = 1$ and $\lambda = 1$ in both the dry and wet formulas, and ignore the wet effects, then we obtain Black's single-term mapping function to a good degree of approximation.